Spin-orbit interaction and phase coherence in lithographically defined bismuth wires

M. Rudolph and J. J. Heremans

Phys. Rev. B **83**, 205410 — Published 18 May 2011

DOI: 10.1103/PhysRevB.83.205410

Spin-orbit interaction and phase coherence in lithographically defined bismuth wires

M. Rudolph* and J. J. Heremans†
Department of Physics, Virginia Tech, Blacksburg, Virginia 24061, USA
(Dated: March 17, 2011)

We present low temperature magnetoresistance measurements on lithographically defined bismuth wires. The phase coherence time and the spin-orbit scattering time are obtained by analysis of weak-antilocalization, with values for the phase coherence time supported by analysis of the universal conductance fluctuations present in the wires. We find that the phase coherence time is dominated by electron-phonon scattering above ≈ 2 K and saturates below that temperature, with saturation delayed to a lower temperature in wider wires. The spin-orbit scattering time shows a weak temperature dependence above 2 K, and also shows a dependence on wire width. The spin-orbit scattering time increases as the width is reduced, as also observed in wires fabricated from spin-orbit coupled two-dimensional systems in semiconductor heterostructures. The similarity is discussed in the light of weak-antilocalization in the two-dimensional strongly spin-orbit coupled Bi(001) surface states.

PACS numbers: 73.63.Nm, 72.25.Rb, 73.23.-b, 73.20.Fz, 73.50.Jt

I. INTRODUCTION

The semimetal bismuth has long been an important material for observing quantum properties, for instance supporting the first experimental observation of magnetic quantum oscillations[1]. Interest in Bi originates from its highly anisotropic electron Fermi surface, characterized by a low carrier density and a long mean free path, moreover possessing large spin-orbit interaction (SOI), rendering it an excellent platform for observing quantum transport in the strong SOI regime. Quantum transport in Bi films has been extensively studied[2–9] as have been self-assembled wires[10–15]. In particular, spin-dependent quantum transport in the form of weak-antilocalization has been observed in Bi films[3–9] and a nanowire array[14]. However, quantum transport in purpose-designed Bi thin film mesoscopic geometries has not enjoyed equal attention[3,17] and lags behind achievements in semiconductor heterostructures[18]. Here we present quantum interference phenomena observed in Bi mesoscopic wires lithographically defined on Bi thin films. The data on single wires with defined dimensions and surface orientation is complementary to previous studies[14–16], and allows us to extract the phase coherence time τ_ϕ and the spin-orbit scattering time τ_{so} to discuss their temperature (T) and size dependences.

Inelastic scattering processes dominate τ_ϕ, which become increasingly rarer as T decreases, suggesting that τ_ϕ diverges as $T \to 0$. However, experiments often find that at low T, τ_ϕ saturates to a finite value τ_ϕ^0 in many different systems. Saturation has been observed in two-dimensional electron systems (2DESs) in semiconductor heterostructures and wires fabricated from 2DESs[19,20], and in various metal wires and films[19] although not in Bi films[3–7,9]. The origin of τ_ϕ^0 is still debated, with some arguments for magnetic scattering from trace magnetic impurities, electron interaction with long wavelength radiation, and fluctuations in the electromagnetic background[19,21].

The spin-orbit scattering time τ_{so} in solid-state systems results from two different mechanisms: 1) electron scattering off heavy elements with strong SOI, present in heavy metals, and 2) spin decoherence due to structural SOI, as induced by bulk inversion asymmetry in the crystal potential in semiconductors (Dresselhaus SOI[22]) or by effectively asymmetric electron confinement potentials in 2DESs (Rashba SOI[23]). For structural SOI, theory predicts that in quasi-one-dimensional (Q1D) wires, τ_{so} increases with decreasing wire width[24,25], indeed experimentally supported for various 2DESs[20,26–29]. As yet, no similar theoretical predictions exist for SOI due to heavy elements, present in bulk Bi. Nonetheless, τ_{so} in our Bi wires experimentally exhibits an increase with decreasing wire width as observed in Q1D wires on 2DESs, indicating that surface states with structural SOI may contribute substantially to the transport in thin film Bi wires. The Bi(001) surface (hexagonal indexing) has been shown to possess strong Rashba-like SOI due to the asymmetry of the surface confinement potential[30,31] with a Rashba parameter $\alpha_R \approx 0.5$ eVÅ, about an order of magnitude higher than characteristic for semiconductor 2DESs[32].

In the low-T magnetoresistance measurements presented below, two quantum corrections to the classical magnetotransport are present, arising from interference between coherent electron paths: weak-antilocalization (WAL), and universal conductance fluctuations (UCFs). The dependence on T and on wire width of τ_ϕ and τ_{so} are extracted from WAL analysis. We implement analysis of the UCFs to obtain independent values for τ_ϕ, in support of those from WAL analysis.

II. BACKGROUND

Weak-localization phenomena result in a characteristic magnetoresistance at low magnetic fields[33–37] and originate from quantum mechanical interference of backscat-

tered time-reversed paths. For a system with weak SOI ($\tau_{so} \gg \tau_\phi$), the time-reversed paths interfere constructively, resulting in a larger probability for the electrons to be localized, increasing the resistance. For a system with strong SOI ($\tau_{so} \ll \tau_\phi$) the $s = 1/2$ spin symmetry causes a phase shift between the time-reversed paths, leading to destructive interference and decreasing the resistance. The resulting quantum correction to the conductivity under SOI is referred to as WAL. The interference phenomena are sensitive to the preservation of the quantum mechanical orbital and spin phases along the entire path, and hence form a probe of τ_ϕ and τ_{so}. An applied magnetic field B breaks time-reversal symmetry via the addition of an Aharonov-Bohm phase, and the reduction of the WAL correction leads to a characteristic magnetoresistance.

The change in the resistance $\Delta R(T,B) = R(T,B) - R(T,0)$ due to WAL for a 2-dimensional system with SOI can be expressed as[37,38]:

$$\frac{\Delta R(T,B)}{R(T,0)^2} = -\frac{e^2}{2\pi^2\hbar}\frac{W}{L}\left[\frac{3}{2}f(H_3/B) - \frac{1}{2}f(H_2/B) - f(H_1/B)\right], \quad (1)$$

where $f(x) = \Psi(1/2+x) - \ln x$, Ψ represents the digamma function, $H_1 = H_0 + H_{so}$, $H_2 = H_i + 4/3H_{so}$, and $H_3 = H_i$. The characteristic fields $H_{0,i,so}$ relate to scattering times as $H_{0,i,so} = \hbar/(4eD\tau_{0,i,so})$, where τ_0 represents the elastic scattering time derived from the mobility and τ_i the inelastic scattering time. L represents the wire length, W the wire width, and D the carrier diffusion constant. We have ignored terms of magnetic spin-flip scattering, as we do not expect magnetic impurities to be present in the wires[39–42] and thus $\tau_i = \tau_\phi$[19]. The phase and spin coherence lengths are defined respectively as $L_\phi = \sqrt{D\tau_\phi}$ and $L_{so} = \sqrt{D\tau_{so}}$. At low T, τ_ϕ is limited by low-energy transfer Nyquist scattering (characterized by τ_N), and at higher T, by electron-phonon scattering (characterized by τ_{el-ph}). The dependence on T of both scattering mechanisms are modeled as power laws with $\tau_{N,el-ph} \propto T^{-p}$. For Nyquist scattering in 1 dimension[43] $p = 2/3$, in 2 dimensions $p = 1$, and in 3 dimensions[44] $p = 3/2$. The exponent p for electron-phonon scattering is not theoretically agreed upon and has been experimentally determined[19] as $p \approx 2 - 4$.

UCFs arise from interference along non-localized paths from random disorder[45–47] in mesoscopic systems, resulting in deviations from the classical conductance and hence in the resistance R of mesoscopic systems. UCF analysis can yield values for L_ϕ since L_ϕ imposes a limit on the length of the interfering paths. We use the UCF analysis as secondary supporting information to comfirm our WAL analysis. The fingerprint of UCFs in R changes with disorder configuration and general UCF formalisms must involve ensemble averages over samples. Experimentally the impurity configuration can be varied by modifying the interfering paths, accomplished by varying the Fermi level E_F, or by modifying the dynamics of the electron phase, accomplished by applying B and adding an Aharonov-Bohm phase throughout the sample. Averaging over the UCF fingerprints at different E_F or B in one sample is equivalent to averaging the UCF fingerprints over different samples. Varying E_F in metallic Bi is difficult, and hence our study of UCFs proceeds by magnetoresistance measurements. L_ϕ is extracted from the UCF signal by analysis of the autocorrelation in B of $R(B)$. From the autocorrelation function $F(\Delta B) = \langle \delta R(B)\delta R(B+\Delta B)\rangle$ we extract a correlation field B_c such that $F(\Delta B_c) = 1/2F(0)$. The angled brackets denote averaging over B. B_c provides a measure of the average length of interfering paths, since long paths require smaller B to decorrelate by the accumulated Aharonov-Bohm phase. In Q1D wires, B_c and L_ϕ are related by[47]:

$$B_c = C\frac{h}{e}\frac{1}{L_\phi^2}, \quad L_\phi < W, \quad (2)$$

where $C = 0.95$ for $L_\phi \gg L_T$ and $C = 0.45$ for $L_\phi \ll L_T$[48].

III. EXPERIMENT

Bismuth thin films were grown by thermally evaporating Bi (99.999%) onto a SiO_2 (oxidized Si(001)) substrate under vacuum below 10^{-8} Torr. A two step evaporation was implemented to obtain films with the largest grain sizes and fewest defects[2,17]. First, a 20 nm thick layer was evaporated at a rate of 0.1 nm/s onto a 100°C substrate. The substrate was then further heated to 250°C, and a 55 nm thick layer was deposited, also at a rate of 0.1 nm/s. The evaporation rate and film thickness were monitored by a quartz balance crystal monitor to an accuracy of $< 5\%$. Atomic force microscopy revealed grains with diameters of 200-500 nm and a total film thickness t of 75 nm. X-ray diffraction analysis specified that the films are oriented with their trigonal axis (001) perpendicular to the substrate, typical for our growth methods. This places the three anisotropic electron pockets in the plane of the film and the single hole pocket perpendicular to the film. The in-plane orientation is random.

A two step lithography was used to pattern mesoscopic wires onto the Bi film. First, a 50 μm wide, multiterminal Hall bar mesa was photolithographically defined on the film. The exposed Bi was etched with a solution of H_2SO_4:H_2O_2:H_2O. Second, wires of lithographic width 7 μm and 15 μm were patterned from the mesa using the same wet etchant after electron beam lithography. Wire width was controlled by laterally overetching the Bi thin film in the second step, obtaining physical widths W of 0.34 μm and 6.1 μm respectively for the two wires, with common length of 22 μm. The inset of Fig. 1 contains a SEM micrograph of the wires. Wood's metal contacts were applied to the mesa for electrical characterization.

Magnetotransport measurements were performed in a ^{3}He cryostat down to T=400 mK, using standard lock-

in techniques. The film's carrier mobilities and densities were determined from magnetoresistance and Hall data. We fit the data to an isotropic three-carrier model, which takes into account the two expected bulk bands as well as an impurity band from the initial 20 nm of Bi growth. For the bulk bands, $n_b = 2.5 \times 10^{23}$ m^{-3}, $\mu_b = 0.28$ m^2/Vs, $p_b = 1.4 \times 10^{23}$ m^{-3}, and $\nu_b = 0.39$ m^2/Vs, where n (p) and μ (ν) are the density and mobility of the electrons (holes). The impurity band is n-type with $n_{imp} = 6 \times 10^{26}$ m^{-3} and $\mu_{imp} = 7 \times 10^{-4}$ m^2/Vs. The densities and mobilities of the bulk bands are similar to those observed in single crystalline Bi films[2]. However, since WAL measurements cannot differentiate between contributions from the different carriers, for the analysis we use a two-carrier fit, where $n = 8.8{\times}10^{24}$ m^{-3} and $\mu = 0.056$ m^2/Vs, $p = 2.5 \times 10^{23}$ m^{-3}, and $\nu = 0.36$ m^2/Vs. Shubnikov-de Haas oscillations were not present for magnetic fields up to 9 T, due to the Fermi surface averaging over many randomly oriented grains. The resistivity ρ_0 of the film at 0.4 K is 1.1×10^{-5} Ωm. The cross section of the hole Fermi surface is isotropic in the plane of the film, and hence ν represents the true hole mobility. The electrons, however, are confined to three anisotropic Fermi surfaces, and μ then represents an effective transport mobility through many randomly oriented grains. In pure crystalline Bi, the electron and hole densities should be equal due to charge neutrality[49,50]. Our films are slightly n-doped, likely a result of lattice strain and vacancies due to the substrate mismatch and polycrystalinity. The resistivities (0.4 K) of the 6.1 μm and 0.34 μm wide wires are both 1.0×10^{-5} Ωm, values in good agreement with the unpatterned film. We conclude that densities and mobilities in the wires are not affected by patterning.

Resistance measurements of the 0.34 μm and 6.1 μm wide wires include contact resistances of 2% and 33% respectively, originating in the wide Bi connecting leads. The relative WAL signal as expressed in Eq. 1 is affected proportionally to the contact resistance. However, the parameters τ_ϕ and τ_{so} exctracted from WAL are only weakly dependent on its relative amplitude. While the relative UCF amplitude also is proportionally dependent on contact resistance, B_c again remains unaffected. The effects of contact resistances on the analyses are therefore negligible, and for simplicity ignored.

IV. RESULTS AND DISCUSSION

Figure 1 shows the wire magnetoresistance in a magnetic field perpendicular to the substrate. The data are not offset and indicate a decrease in resistance for increasing temperature, a trend that persists to room temperature. The positive magnetoresistance characteristic of WAL is observed in both the 0.34 μm and 6.1 μm wide Bi wires. UCFs also appear in both wires, particularly visible at $B \approx 0.2$ T and $T < 2$ K in the 0.34 μm wire and, as expected, weaker in the wider wire. The magnitude of both interference effects increases with decreasing

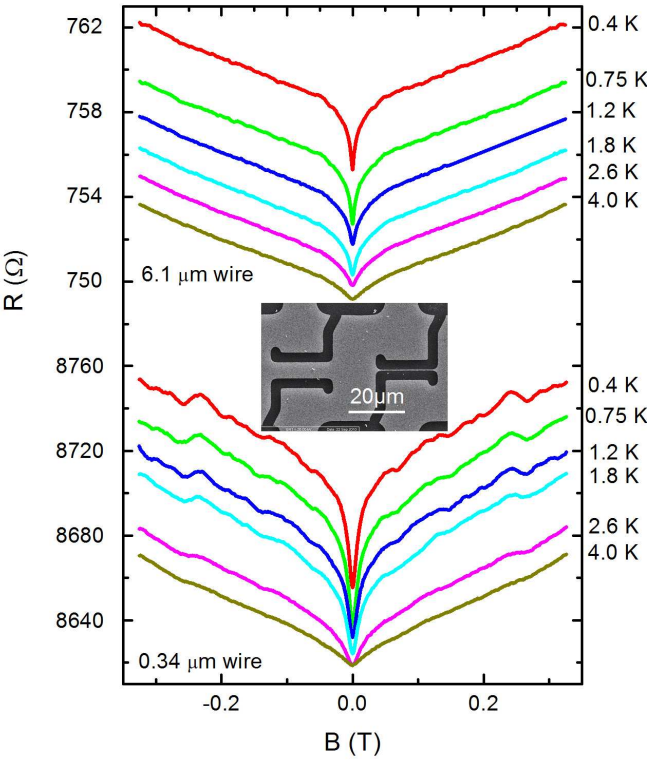

FIG. 1: (Color online)The magnetoresistance in a perpendicular magnetic field of 0.34 μm and 6.1 μm wide lithographically defined Bi wires at T from 0.4 K to 4.0 K. WAL and UCFs are present for both wires. The curves are not offset. Inset: SEM micrograph of the wires, with 20 μm scale bar.

T due to increasing L_ϕ.

The validity of Eq. 1 is dependent on the sample being 2-dimensional concerning phase coherent phenomena, *i.e.* L_ϕ and the magnetic length $L_m = \sqrt{\hbar/eB}$ must exceed the film thickness. At $B = 0.1$ T, $L_m = 80$ nm $\approx t$, and thus performing the fits for $L_m > 2t$ ($|B| < 0.03$ T) preserves the validity of Eq. 1. Using L_ϕ derived from Eq. 1, L_ϕ self-consistently also exceeds t as shown below. The Bi wires, however, are kinematically 3-dimensional, since both the mean free path and Fermi wavelength are smaller than the film thickness, and hence we use $D = v_F^2\tau_0/3$ to obtain the characteristic fields ($H_{0,\phi,so}$), with v_F the Fermi velocity. For the electrons, n and μ yield $\tau_0 = 3.1 \times 10^{-14}$ s and $D = 0.0027$ m^2/s, leaving only τ_ϕ and τ_{so} as fitting parameters to Eq. 1.

Figure 2 displays the low-B magnetoresistance with the best fits from Eq. 1. A small quadratic term was also included in the fit to account for contributions from the classical multi-band magnetoresistance. The terms are $265(\Omega/\mathrm{T}^2)B^2$ (0.34 μm wire) and $25(\Omega/\mathrm{T}^2)B^2$ (6.1 μm wire). For both wires, the correction corresponds to $\rho(B) = \rho_0(1 + 0.18(\mathrm{T}^{-2})B^2)$, which is a few orders of magnitude lower than that of single crystal bulk Bi due

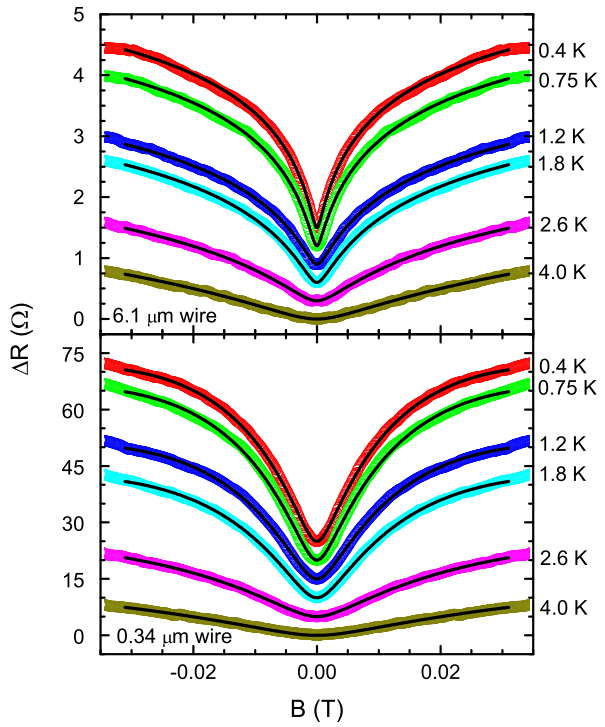

FIG. 2: (Color online) Low-B magnetoresistance data (circles) at variable T for Bi wires of widths 0.34 μm and 6.1 μm. The black lines represent fits to Eq. 1 with τ_ϕ and τ_{so} as fitting parameters. Data are offset for clarity.

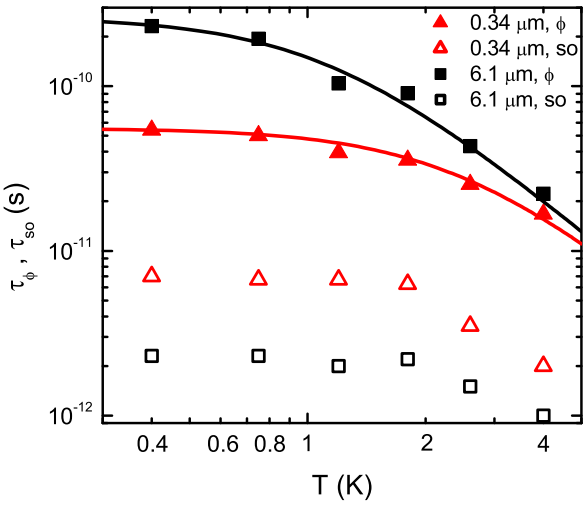

FIG. 3: (Color online) The phase coherence time τ_ϕ and the spin coherence time τ_{so} extracted from WAL. The solid lines represent fits to Eq. 3 with τ_ϕ limited by electron-phonon scattering over the range of T considered here.

to a reduction in mobility for thin films[2] and the polycrystalline nature of our films.

Figure 3 depicts the dependence on T of the extracted parameters τ_ϕ and τ_{so}. The corresponding coherence lengths L_ϕ and L_{so} are provided in Fig. 5. The T-dependence of τ_ϕ weakens with decreasing T, indicative of saturation and of an intrinsic T-independent phase decoherence mechanism. Saturation of τ_ϕ has been widely observed[19,20] in 2-dimensional samples and nanostructures in both semiconductors and metals, but as yet not in Bi.

Adding a saturating term to the power-law T-dependence of τ_ϕ yields[19]:

$$\frac{1}{\tau_\phi} = \frac{1}{\tau_\phi^0} + AT^p. \qquad (3)$$

The solid lines in Fig. 3 represent fits to Eq. 3 including saturation for τ_ϕ. From the fit, $\tau_\phi^0(0.34\ \mu\text{m}) = 5.5 \times 10^{-11}$ s and $\tau_\phi^0(6.1\ \mu\text{m}) = 2.6 \times 10^{-10}$ s, indicating that the thinner wire experiences saturation more strongly. The exponent $p = 2$ provides the best fit, corresponding to inelastic decoherence due to electron-phonon scattering. The coefficient $A = 2.9 \times 10^9$ K^2/s is found equal for both wires, indicating decoherence by low energy phonons unaffected by W. Nyquist phase decoherence, characterized by τ_N, is not observed since fitting to $\tau_\phi^{-1} = \tau_N^{-1} + \tau_{el-ph}^{-1}$ instead of Eq. 3 does not provide convincing fits[51]. The saturation term masks Nyquist decoherence in the region $T < 1$K where the Nyquist mechanism would otherwise dominate.

The data reveal a dependence on W for τ_ϕ via τ_ϕ^0. Many experiments have shown a dependence of τ_ϕ^0 on the disorder in the system, characterized by D[52–54]. A dependence of D on W is detectable by a change in resistivity with W. In the present work resistivity values in the wires and film are comparable, indicating a constant D unaffected by processing the thin film into wires. Further, a size dependence of the saturation term τ_ϕ^0 has previously been reported in Au wires,[55] where thinner wires saturate at a lower T and show longer τ_ϕ^0 than wider wires. Our Bi wires are in a very different size and disorder regime from the Au wires, and we observe an opposite effect. We attribute the dependence on the mesoscopic dwell time. In ballistic quantum dots, a size dependence of τ_ϕ^0 has been attributed to the dwell time $\tau_d = Sm^*/\hbar N$ in the dot, where S represents the area of the dot, m^* the effective mass, and N the number of conducting channels entering/exiting the dot[56]. In our case, W acts as limiting dimension for τ_d, leading to a dependence on W in qualitative agreement with the experimental result.

At low T, theory predicts a τ_{so} independent of T. In the Bi wires, as depicted in Fig. 3, the extracted τ_{so} exhibits a slight but noticeable dependence on T above $T \approx 1.8$ K. We note that at 3.6 K, the thermal diffusion length $L_T = \sqrt{\hbar D/k_B T}$ equals the film thickness, and hence an effective change in dimensionality of the system may underlie the apparent dependence on T not captured

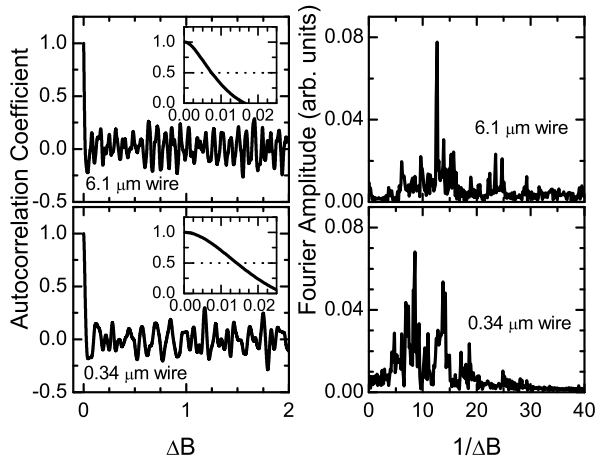

FIG. 4: The left hand panels are the autocorrelation function of the UCFs in the 0.34 and 6.1 μm Bi wires at 0.4 K. The inset shows the decay of the autocorrelation function at small ΔB. The right hand panels are the Fourier transforms of the autocorrelation functions.

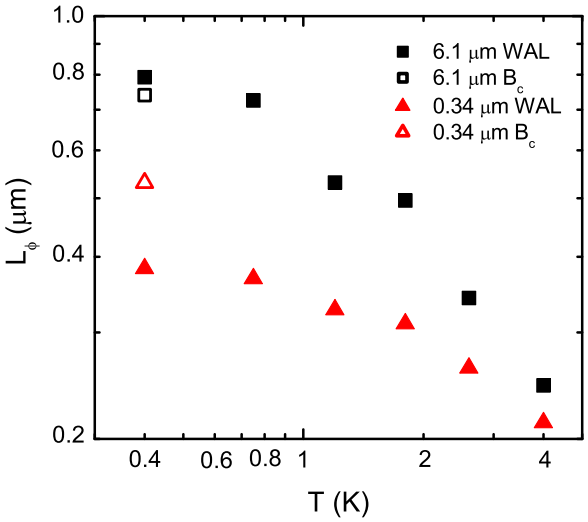

FIG. 5: (Color online) Phase coherence lengths L_ϕ as function of T in Bi wires, comparatively derived from WAL and UCF autocorrelations.

in Eq. 1. Further, τ_{so} increases as W decreases. In semiconductor 2DESs, where the SOI is dominated by inversion asymmetry via the structural Rashba and Dresselhaus terms, experiments and theory have verified[20,24–29] that $\tau_{so} \propto W^{-1/2}$. A similar dependence has not been proposed in the 3-dimensional bulk for SOI in heavy metallic elements like Bi. Thus, we note that both the bulk band and impurity band cannot account for the W-dependence due to their 3-dimensional character. The similarity however of our present observations of a W-dependent τ_{so} with results from semiconductor 2DES wires suggests a large contribution to the transport from Bi surface states with structural SOI. It is known that self-assembled Bi nanowires can show transport contributions from surface states[16]. Specifically, the Bi(001) surface exhibits strong Rashba-like SOI from the asymmetric surface confinement potential[31], and also represents the dominant surface area in our wires fabriated from (001)-oriented films. Our observations can hence find an explanation assuming a transport contribution from surface states with strong Rashba-like SOI.

UCFs are present in both Bi wires, as depicted in Fig. 1. Analysis on the UCFs provides an independent consistency check for the τ_ϕ extracted by WAL. The left panels of Fig. 4 show the autocorrelation $F(\Delta B)$ of the UCFs up to $\Delta B = 2$ T at T=0.4 K. UCF analysis requires detailed data over a large magnetic field range, and therefor only data for the lowest temperature was taken, where UCFs are most prominent. The insets provides a magnified view at low ΔB to indicate the decay of the autocorrelation function, from which B_c can be determined. The insets in Fig. 4 indicate $B_c(0.34\ \mu\text{m}) = 0.014$ T and $B_c(6.1\ \mu\text{m}) = 0.0075$ T, corresponding to $L_\phi(0.34\ \mu\text{m}) = 0.53\ \mu$m and $L_\phi(6.1\ \mu\text{m}) = 0.74\ \mu$m according to Eq. 2. The values of L_ϕ determined from WAL and from the low-ΔB analysis of $F(\Delta B)$ are in reasonable agreement (within $\sim 30\%$) and are collected in Fig. 5.

For randomly disordered systems, $F(\Delta B)$ is expected to decay to zero at high ΔB. However, oscillations persist to high ΔB in Fig. 4, the result of few but dominant scattering centers superposed on the random disorder. The right panels contain the Fourier transforms of $F(\Delta B)$, indicating the existence of well-defined periodicities in ΔB. The periodicities form the magnetofingerprint of dominant scattering centers which generate circling interfering carrier paths with corresponding h/e Aharonov-Bohm flux periodicities. Both wires show comparable ΔB periodicities, indicating that the concomitant fluctuations in R do not form part of the averaged UCF signature, but rather originate in orbits dominating equally for different sized samples. It is likely that the orbits pertain to scattering around misoriented grains, expected to be of equal size in both wires. For the electrons to show the defined periodicities of Fig. 4, they must traverse a minimum distance of $\sim \pi r$ where $\pi r^2 (1/\Delta B)^{-1} = h/e$. For the two dominant periodicities in the 0.34 μm wire, the path lengths amount to 0.33 μm and 0.42 μm. The 6.1 μm wire shows one dominant periodicity corresponding to a path length of 0.41 μm. The path lengths fall within L_ϕ, consistent with the WAL analysis and the low-ΔB analysis of $F(\Delta B)$.

V. CONCLUSIONS

The temperature dependence and width dependence of τ_ϕ and τ_{so} in lithographic Bi wires (widths of 0.34 μm

and 6.1 μm) with (001) surface orientation are investigated by the weak-antilocalization and universal conductance fluctuation phenomena. Electron-phonon interactions dominate τ_ϕ above 2 K, with an interaction strength of $A = 2.9 \times 10^9$ K^2/s for both wires. Both wires exhibit a low-temperature saturation of τ_ϕ, with the wider wire saturating at a lower temperature. The extrapolated phase coherence saturation times are found as $\tau_\phi^0(0.34\ \mu\text{m}) = 5.5 \times 10^{-11}$ s and $\tau_\phi^0(6.1\ \mu\text{m}) = 2.6\times10^{-10}$ s. The spin-orbit scattering times show a weak temperature dependence above 2 K. A width dependence of τ_{so} is also observed, where the wider wire exhibits a shorter τ_{so}, similar to observations in semiconductor 2DES wires. The width dependence of τ_{so} indicates a similarity between transport in lithographically defined Bi wires and semiconductor 2DES wires, suggesting that the weak-antilocalization signature in Bi wires is dominated by Bi(001) surface states with strong Rashba-like SOI. This corroborates recent observations of strongly spin-orbit split bands on Bi(001) by ARPES experiments. Isolating magnetotransport features of the Bi(001) surface forms a promising avenue to study phenomena at large SOI, due to a comparatively simple growth procedure and lithographic flexibility to pattern mesoscopic structures on Bi thin films.

Acknowledgements

The authors would like to thank V. Soghomonian for detailed discussions and C. S. Park for XRD on the Bi films. This work was supported by the DOE through Grant No. DOE DE-FG02-08ER46532.

* Electronic address: rudolphm@vt.edu
† Electronic address: heremans@vt.edu

[1] P.L. Kapitza, Proc. R. Soc. London Ser. A **119**, 358 (1928).
[2] D.L. Partin, J. Heremans, D.T. Morelli, C.M. Thrush, C.H. Olk, and T.A. Perry, Phys. Rev. B **38**, 3818 (1988).
[3] D.E. Beutler and N. Giordano, Phys. Rev. B **38**, 8 (1988).
[4] D.S. McLachlan, Phys. Rev. B **28**, 6821 (1983).
[5] P.H. Woerlee, G.C. Verkade, and A.G.M. Jansen, J. Phys. C: Solid State Phys. **16**, 3011 (1983).
[6] Yu.F. Komnik, E.I. Bukhshtab, V.V. Andrievskii, A.V. Butenko, J. Low Temp. Phys. **52**, 315 (1983); E.I. Bukhshtab, A.V. Butenko, Yu.F. Komnik, and V.V. Pilipenko, Solid State Comm. **53**, 347 (1985).
[7] Yu.F. Komnik, V.Yu. Kashirin, B.I. Belevtsev, and E.Yu. Beliaev, Phys. Rev. B **50** 15298 (1994); V.Yu. Kashirin and Yu.F. Komnik, Phys. Rev. B **50**, 16845 (1994).
[8] Yu.F. Komnik, I.B. Berkutov, and V.V. Andrievskii, Fiz. Nitzk. Temp. **31**, 429 (2005) [Low Temp. Phys **31**, 326 (2005)].
[9] F. Komori, S. Kobayashi, and W. Sasaki, J. Phys. Soc. Jpn. **52**, 368 (1983).
[10] J.P. Heremans, C.M. Thrush, Z.B. Zhang, X. Sun, M.S. Dresselhaus, J.Y. Ying, and D.T. Morelli, Phys. Rev. B **58**, R10091 (1998); Z.B. Zhang, X. Sun, M.S. Dresselhaus, J.Y. Ying, and J. Heremans, Phys. Rev. B **61**, 4850 (2000).
[11] K. Hong, F.Y. Yang, K. Lui, D.H. Reich, P.C. Searson, C.L. Chien, F.F. Balakirev, and G.S. Boebinger, J. Appl. Phys. **85**, 6184 (1999).
[12] W. Shim, J. Ham, J. Kim, and W. Lee, Appl. Phys. Lett. **95**, 232107 (2009).
[13] M. Murata, D. Nakamura, Y. Hasegawa, T. Komine, T. Taguchi, S. Nakamura, C.M. Jaworski, V. Jovovic, and J.P. Heremans, J. Appl. Phys. **105**, 113706 (2009); Y. Hasegawa, M. Murata, D. Nakamura, T. Komine, T. Taguchi, and S. Nakamura, J. Appl. Phys. **105**, 103715 (2009).
[14] T.E. Huber and M.J. Graf, Phys. Rev. B **60**, 16880 (1999).
[15] T.E. Huber, K. Celestine, and M.J. Graf, Phys. Rev. B **67**, 245317 (2003); A. Nikolaeva, D. Gitsu, L. Konopko, M.J. Graf, and T.E. Huber, Phys. Rev. B **77**, 075332 (2008); T.E. Huber, A. Nikolaeva, L. Konopko, M.J. Graf, Phys. Rev. B **79**, 201304(R) (2009).
[16] T.E. Huber, A. Nikolaeva, D. Gitsu, L. Konopko, C.A. Foss Jr., M.J. Graf, Applied Phys. Lett. **84**, 1326 (2004).
[17] B. Hackens, J.P. Minet, S. Faniel, G. Farhi, C. Gustin, J.P. Issi, J.P. Heremans, and V. Bayot, Phys. Rev. B **67**, 121403 (2003).
[18] C.W.J. Beenakker and H. van Houten, Solid State Physics **44**, 1 (1991).
[19] J.J. Lin and J.P. Bird, Journ. Phys.: Condens. Matter **14**, R501 (2002).
[20] R.L. Kallaher, J.J. Heremans, N. Goel, S.J. Chung, M.B. Santos, Phys. Rev. B **81**, 035335 (2010).
[21] P. Mohanty, E.M.Q. Jariwala, and R.A. Webb, Phys. Rev. Lett. **78**, 3366 (1997).
[22] G. Dresselhaus, Phys. Rev. **100**, 580 (1955).
[23] E.I. Rashba, Fiz. Tverd. Tela **2**, 1224 (1960) [Sov. Phys. Solid State **2**, 1109 (1960)].
[24] A.A. Kiselev and K.W. Kim, Phys. Rev. B **61**, 13115 (2000).
[25] S. Kettemann, Phys. Rev. Lett. **98**, 176808 (2007).
[26] A.W. Holleitner, V. Sih, R.C. Myers, A.C. Gossard, and D.D. Awschalom, Phys. Rev. Lett. **97**, 036805 (2006).
[27] Y. Kunihashi, M. Kohda, and J. Nitta, Phys. Rev. Lett. **102**, 226601 (2009).
[28] P. Lehnen, T. Schäpers, N. Kaluza, N. Thillosen, and H. Hardtdegen, Phys. Rev. B **76**, 205307 (2007).
[29] T. Schäpers, V.A. Guzenko, M.G. Pala, U. Zülicke, M. Governale, J. Knobbe, and H. Hardtdegen, Phys. Rev. B **74**, 081301(R) (2006).
[30] C.R. Ast and H. Höchst, Phys. Rev. B **66**, 125103 (2002).
[31] Yu.M. Koroteev, G. Bihlmayer, J.E. Gayone, E.V. Chulkov, S. Blügel, P.M Echenique, and P. Hofmann, Phys. Rev. Lett. **93**, 046403 (2004).
[32] M. Kohda, T. Bergsten, and J. Nitta, J. Phys. Soc. Jpn. **77** 031008 (2008).
[33] E. Abrahams, P.W. Anderson, D.C. Licciardello, and T.V. Ramakrishnan, Phys. Rev. Lett. **42**, 673 (1979).
[34] P.W. Anderson, E. Abrahams, and T.V. Ramakrishnan, Phys. Rev. Lett **43**, 718 (1979).
[35] L.P.Gorkov, A.I. Larkin, and D.E. Khmel'nitzkii, Sh. Eksp. Teor. Fiz. Pis'ma Ref **30**, 248 (1979) [JETP Lett. **30**, 228 (1979)]
[36] B.L. Al'tshuler, D.E. Khmel'nitzkii, A.I. Larkin, and P.A. Lee, Phys. Rev. B **22**, 5142 (1980).
[37] S. Hikami, A.I. Larkin, and Y. Nagaoka, Prog. Theor. Phys. **63**, 707 (1980).
[38] Theoretical expressions involve conductances, while our experiments measure resistances. Thus, all conductance expressions have been linearized to relative changes in resistances, introducing only negligible deviations.
[39] C. Van Haesendonck, J. Vranken, and Y Bruynseraede, Phys. Rev. Lett. **58**, 1968 (1987).
[40] W. Wei and G. Bergmann, Phys. Rev. B **37**, 5990 (1988).
[41] H. Beckmann and G. Bergmann, Phys. Rev. B **54**, 368 (1996).
[42] R.P. Peters, G. Bergmann, and R. M. Mueller, Phys. Rev. Lett. **60**, 1093 (1988).
[43] B.L. Al'tshuler, A.G. Aronov, and D.E. Khmel'nitzkii, J. Phys. C **15**, 7367 (1982).
[44] A. Schmid, Z. Phys. **271**, 251 (1974).
[45] P.A. Lee and A.D. Stone, Phys. Rev. Lett. **55**, 1622 (1985).
[46] P.A. Lee, Physica A **140**, 169 (1986).
[47] P.A. Lee, A.D. Stone, and H. Fukuyama, Phys. Rev. B **35**, 1039 (1987).
[48] C.W.J. Beenakker and H. van Houten, Phys. Rev. B **37**, 6544 (1988).
[49] R.N. Zitter, Phys. Rev. **127**, 1472 (1962).
[50] R. Hartman, Phys, Rev. **181**, 1070 (1969).
[51] S. Wind, M.J. Rooks, V. Chandrasekhar, and D.E. Prober, Phys. Rev. Lett. **57**, 633 (1986).
[52] J.J. Lin and L.Y. Kao, J. Phys.: Condens. Matter **13**, L119 (2001).
[53] J.J. Lin Y.L. Zhong, and T.J. Li, Europhys. Lett. **57**, 872 (2002).
[54] Y. Niimi, Y. Baines, T. Capron, D. Mailly, F.Y. Lo, A.D. Wieck, T. Meunier, L. Saminadayar, and C. Bäuerle, Phys. Rev. Lett. **102**, 226801 (2009).
[55] D. Natelson, R.L. Willett, K.W. West, and L.N. Pfeiffer, Phys. Rev. Lett. **86**, 1821 (2001).
[56] B. Hackens, S. Faniel, C.Gustin, X. Wallart, S. Bollaert, A. Cappy, and V. Bayot, Phys. Rev. Lett. **94**, 146802 (2005).